Vietnam Academy of Science and Technology
Vietnam Journal of Marine Science and Technology
journal homepage: vjs.ac.vn/index.php/jmst

Grain-size distribution characteristics of sediments in coastal shallow waters from Van Don to Tien Yen - Ha Coi, Northwest Gulf of Tonkin, Vietnam, according to End-member modelling analysis

Le Duc Anh[1], Mai Duc Dong[1,*], Tran Thi Thuy Huong[1], Le Duc Luong[2], Nguyen Nhu Trung[1], Vu Hai Dang[1], Bui Van Nam[1], Pham Thu Hien[1], Duong Van Hao[3], Nguyen Anh Minh[4]

[1]*Institute of Marine Geology and Geophysics, VAST, Vietnam*
[2]*Institute of Geological Sciences, VAST, Vietnam*
[3]*VNU School of Interdisciplinary Studies, Vietnam National University, Hanoi, Vietnam*
[4]*UWC Changshu China, No. 88 Kun-Cheng-Hu-Xi Road, Changshu, Jiangsu, China*

Received: 21 October 2023; Accepted: 19 January 2024

ABSTRACT

The study involved the collection of eighteen surface sediment samples from the coastal shallow water area from Van Don to Tien Yen - Ha Coi in the Northwestern section of the Gulf of Tonkin to analyze their particle size composition. Utilizing the EMMAgeo end-member analysis model, four characteristic particle sizes (4EM) of 0.34, 7.7, 130, and 230 µm, corresponding to clay, fine silt, and fine sand of varying sizes were identified. In conjunction with the sedimentary environment, the spatial distribution analysis of these end members allowed a detailed determination of the formation conditions and distribution of the sediment components. Clay deposits (EM1) are primarily intercalated between the islands. At the same time, fine silt (EM2) is concentrated in the northern part of the study area, transported by flows, and deposited in a low-energy environment. Fine sand sediments (EM3 and EM4) are distributed along the coast of the Van Don peninsula in the Southern part of the study area and likely formed in association with tidal-wave processes under higher energy conditions compared to the North.

Keywords: Grain-size, end-member modelling analysis, linear discriminate function, Gulf of Tonkin.

[*]Corresponding author at: Institute of Marine Geology and Geophysics, 18 Hoang Quoc Viet, Cau Giay, Hanoi, Vietnam.
E-mail addresses: ducdong.geo@gmail.com

https://doi.org/10.15625/1859-3097/18898
ISSN 1859-3097; e-ISSN 2815-5904/

INTRODUCTION

Changes in coastal sediment characteristics result from variations in natural conditions and (or) anthropogenic impacts at local, regional, and global scales, spanning from months to thousands of years and more [1–2]. Studies on sediments in coastal areas indicate that alterations in petrographic, geochemical, and biochemical compositions are regular due to being influenced by material supply, river sediment transport, topographical and geomorphological features, oceanographic factors, and climate change [3–11]. Although coastal sediments are only partially retained from the primary source, they are frequently regarded as the foundation for theoretical interpretation when reconstructing environmental changes that have occurred during past periods [12–17]. In most cases, sediment obtained from the seafloor surface results from a combination of interacting processes. Therefore, a prerequisite for studying changes in sediment properties over time is understanding the causes of spatial sediment changes in the present before making assessments regarding long-term regular changes [9, 18–21].

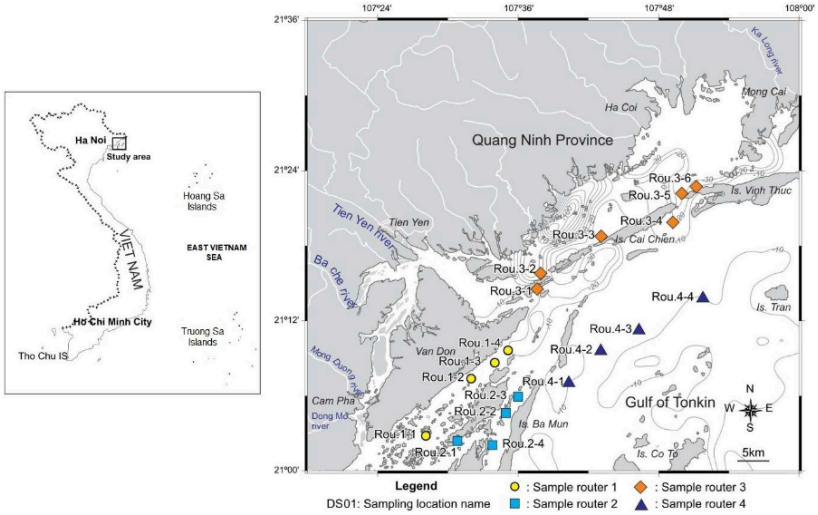

Figure 1. Map of the study area and sampling sites

Grain size distribution and the parameters and shape of grain size distribution curves are closely linked to sediments' transport mechanism and size-sorting processes within specific deposition environments [22]. Generally, sediments are mixtures of two or more particle components with varying origins and transport processes [23]. Traditional statistical approaches that describe mean grain size, standard deviation, or selectivity need to improve the interpretation of information related to sedimentary processes [24]. Therefore, from a mathematical and statistical perspective, Weltje (1997), Weltje and Prins (2003) [25] proposed the End-Member Modeling Analysis (EMMA) method to analyze sediment grain size distribution, aiming to extract information about the origin, transport method, and sediment deposition environment. Since then, EMMA methods have been developed and widely

applied in various regions worldwide. In essence, end-member modeling is a valuable tool that may unveil sedimental inputs to a system that cannot be determined solely via univariant particle parameters [26]. EMMAgeo, one of these methods, has demonstrated its suitability and efficacy through numerous studies conducted in different areas, typically the Donggi Cona Lake area in the northeastern Tibetan Plateau, China [18, 27]; the Heuksan area in southwest Korea [28]; the Western Alboran Sea [29]; the Hai Hau area in Vietnam [30]; and the Taiwan Strait area [31]. This study applies the EMMAgeo method to identify the dominant sediment particle size groups and interpret them based on hydrodynamic characteristics to clarify the dynamics of sediment transport and accumulation in the study area (Figure 1).

The study area encompasses the shallow water region along the coast, extending from Van Don to Tien Yen - Ha Coi, in the northwest part of the Gulf of Tonkin. It is adjacent to Mong Cai City in the northeast, Bai Tu Long Bay, and Ha Long Bay in the southwest, and borders Co To Island district to the east. This area features a complex bottom topography due to its surroundings of large and small islands formed from various types of ancient sedimentary rocks. Regional sediments comprise five main groups, ranging from very fine to coarse grains, including gravelly sand, gravelly mud, sand, mud, and sandy mud [32–33]. These sediments have complex characteristics, distribution patterns, material sources, and sediment deposition environments.

Study area

The study area is within the Gulf of Tonkin, characterized by a tropical monsoon climate typical of northern Vietnam. It experiences two distinct seasons. The hot and humid weather in the summer accompanied by abundant rainfall. During this time, prevailing wind directions originate from the east, southeast, and south, with average wind speeds ranging from 1.6 to 3.5 m/s. On the other hand, the winter season is characterized by dry and cold conditions with low precipitation levels. The dominant wind directions during this time are Northeast, North, and East at an average rate of 1.9 and 3.1 m/s, but other directions are less common. The transition between these two seasons occurs in April and October [34–35]. This region experiences a high concentration of storms compared to other coastal areas in Vietnam. Typhoons frequently occur during the summer months, depending on the movement of the tropical convergence band [36].

Freshwater flows into Bai Tu Long Bay primarily from four main rivers: the Tien Yen River, the Ba Che River, the Mong Duong River, and the Dong Mo River. Among these, the Tien Yen River is the largest, covering a basin area of 1,070 km^2. The other rivers, with smaller basins, include the Ba Che River, the Mong Duong River, and the Dong Mo River, each with an area of less than 100 km^2 [34]. The volume of water from these rivers varies with the seasons. During the flood season (from May to September), it constitutes 75–80% of the total annual water volume, whereas the dry season, from October to April of the following year, accounts for 20–25% of the yearly total. In the dry season, the primary water source for the rivers includes groundwater, and a smaller amount is supplemented by rain brought on by the variable Northeast monsoon [34].

The monsoon regime primarily influenced. At the Hon Gai station, located inside Ha Long Bay, the average wave field records waves at a height of 0.1 m with a wave period of 1.5 seconds [35]. Bai Tu Long Bay, covered mainly by islands, is less affected by deep water wave fields, resulting in generally weak waves throughout the year. In contrast, the area outside Bai Tu Long Bay, which is the open seas, tightly depends on the wind regime, and as such, wave patterns experience significant seasonal variation. During the winter, waves originate predominantly from the Northeast (40%), followed by the North and East, with wave tranquillity accounting for roughly 10%. Average wave height in winter ranges from 1 to 1.5 m. In the summer, waves from Southeast and Southwest alternate to be predominant, collectively representing about 60% of the total frequency, and tranquillity constitutes around 20%, with average wave height being approximately 1 m [34].

The tide in the study area follows a diurnal tidal regime, with tidal magnitude gradually decreasing from North to South. The maximum tide level reaches 4.67 m, while the average tide stands at 2.15 m. The highest tides occur during June-July and October-December, with water levels rising at a rate of up to 0.5 meters per hour. Diurnal fluctuations are observed, and ebb tide durations are typically shorter than high tide durations [34, 37]. While tidal residuals can be locally strong, they generally remain weaker than wind-driven currents, particularly during the winter monsoon [38].

The flow within the study area is closely connected to the circulation of the Gulf of Tonkin, where both winter and summer witness the presence of a cyclonic, with its center positioned in the middle of the Gulf of Tonkin. This center undergoes a southward shift during winter, whereas it experiences a northward movement during the summer. Because of its location along the western periphery of this circulation, there is a consistent current flow from North to South along the shoreline in both seasons. However, due to the intricate topography of this marine region, the surface flow direction changes considerably between different locations. The average flow speed measures between 20 and 25 cm/s. The numerous sea bays in the region, shielded by islands, contribute to the complexity of the flow, with tidal currents and seabed topography playing a predominant role. Notably, the flow rate increases dramatically when passing through narrow straits and inlets between islands, with velocities reaching around 100 cm/s [36]. In terms of sediment accumulation in the vicinity of the study area, it is relatively slow, with values ranging from 0.47 to 0.75 cm/year, as determined through isotope age analysis involving ^{210}Pb and ^{137}Cs [39].

Material and method

In the dry season 2022, eighteen surface sediment samples (0–5 cm per column) were collected using a gravity core. Sampling took place in four distinct areas/lines, namely: 1) the coastal area along the Van Don peninsula (area 1); 2) the region between Tra Ngo and Ba Mun Islands (area 2); 3) the area adjacent to Cai Chien and Vinh Thuc Islands, where the Tien Yen Estuary meets the sea; and 4) the shallow sea area beyond the islands (Figure 1).

Surface sediment samples collected from the core's top (0–5 cm) were treated with HCl and H_2O_2 to eliminate carbonate and organic matter. Subsequently, these samples were analyzed using a Horiba LA960 instrument, which has a measuring range spanning from 0.01 µm to 5,000 µm (11φ - 2.5φ). Particle size parameters, including mean (M), sorting (σ), skewness (Sk), and kurtosis (K), were calculated in micrometers (µm) and phi (φ) units. These calculations were performed following the equations established by Folk and Ward (1957) and were processed using the GRADISTAT v9.1 program. The results are presented in Supplementary Table 1.

The Linear Discriminate Function (LDF) is employed to learn about alterations in physical conditions during sediment deposition according to Sahu (1964) [5] and subsequently modified by Baiyegunhi et al., (2020) [10]. The distinction in sediment accumulation environments is determined based on four fundamental equations: Y_1, Y_2, Y_3, and Y_4. These equations are calculated using granularity parameters M, σ, Sk, and K, with the calculation formulas provided in Table 1. The calculation results are presented in Supplementary Table 2.

The EMMAgeo method published by Dietzel E. and Dietzel M. in 2019 [40] is used with seven calculation steps, including:

Step 1: Transforming grain size data formats to a constant sum (1 or 100%).

Step 2: Rescaling and standardizing. Applying column-wise weight transformation creates a weighted matrix W by expanding the columns based on the percentage P with lower (l) and upper ($100 - l$) bounds:

$$W = (X - h)/(g - h) \quad (1)$$

where vectors h and g are defined by $hj = Pl(xj)$ and $gj = P100 - l(xj)$ for columns j = 1, 2,..., p. A value of l = 0 reflects the minimum and maximum of each column, and for example, a value of l = 2.5 gives percentiles between P2.5/P97.5. For the sake of simplicity,

we set lw = 0.05, however, note that the optimal value l_{opt} is found after iteration stops.

Step 3: Extracting the eigenvector V of the matrix and eigenvalue Λ from the secondary product matrix Γ given by $\Gamma = WTW$ (2).

Step 4: Carrying out the Factor rotation. Applying factor rotation (e.g., *VARIMAX*) on the eigenspace of q end-members in order to simplify the structure of the end-members, thus facilitating factor interpretation. The number of end-members (q) needs to be determined by iteration.

Step 5: Normalizing the preliminary eigenvector loadings (V) to ensure the nonnegativity of the rotated eigenvectors and estimate the eigenvector scores (M) using linear nonnegative least squares as the objective function. This matrix contains the relative contributions of each end-member to each sample. Usually, scores can be interpreted as time series, depth series, or spatial distribution patterns of end-member abundance.

Step 6: Rescaling matrices and computing variance explained. Reversing the initial weight transformation in order to rescale V and M to the original units of the initial data set. Normalizing the rescaled matrices to fulfill the constant sum constraint. The rescaled and standardized matrices are denoted as *end-member loadings* (V^*) and *end-member scores* (M^*), respectively. Calculating the variance, explained by each end-member as the proportion of total scores variance. Scores are the relative contributions of the loadings to a sample and are thus related to the predominance of a process during the formation of the sedimentary deposit.

Step 7: Evaluating goodness of model fit. Calculating the modeled data set $X^* = M * V * T$ (3) and the respective error matrix $E = X^* - X$ (4). Evaluating the goodness of fit by calculating mean row- and column-wise linear coefficients of determinations (r^2) between X and X^*. The resulting matrix gives the explained proportion of variance of each sample and each variable, respectively (Dietzel et al. 2012).

The result of EMMAgeo is a data set, called/understood as end-member, that has all the characteristics of the entire sample set grain size dataset.

Table 1. Classification of sediment deposition environments according to Baiyegunhi et al., (2020) [10]

Environments and processes discrimination	Equation	Indication
Between "shallow agitated water" and "Littoral environment"	$Y_1 = -3.5688M_z + 3.7016\sigma_I^2 - 2.0766Sk + 3.1135K_G$	$Y_1 > -2.7411$ would indicate littoral environment while $Y_1 < -2.7411$ would refer to an shallow agitated water process.
Between "Littoral environment" and "Shallow marine environment"	$Y_2 = 15.6534M_z + 65.7091\sigma_I^2 + 18.1071Sk + 18.5043K_G$	$Y_2 > 63.3650$ would refer to a shallow marine environment $Y_2 < 63.3650$ would indicate littoral environment
Between "Shallow marine environment" and "lacustrine or deltaic"	$Y_3 = 0.2852M_z - 8.7604\sigma_I^2 - 4.8932Sk + 0.0482K_G$	$Y_3 > -7.4190$ would refer to a shallow marine environment $Y_3 < -7.4190$ would indicate a lacustrine or deltaic.
Between "deltaic deposition" and "Turbidity current process"	$Y_4 = 0.7215M_z - 0.4030\sigma_I^2 + 6.7322Sk + 5.2927K_G$	$Y_4 < 9.8433$ would indicate turbidity current process $Y_4 > 9.8433$ would refer to a deltaic deposition process.

Supplementary Table 1. Results of analysis of grain composition and sediment classification. Mean, Sorting, Skewness, Kurtosis values calculated according to Fork and Ward (1957); classification of sediments after Folk (1954)

STT	Sample	Mean (M_G)	Sorting (σ_G)	Skew-ness (Sk_G)	Kurto-sis (KG)	Group (Folk, 1954)	STT	Sample	Mean (M_G)	Sorting (σ_G)	Skew-ness (Sk_G)	Kurto-sis (KG)	Group (Folk, 1954)
1	Rou. 1-1	107.1	5.468	-0.605	0.792	Silty Sand	11	Rou. 3-3	10.98	2.874	0.343	1.537	Sandy Silt
2	Rou. 1-2	49.22	7.842	-0.135	0.882	Sandy Silt	12	Rou. 3-4	118.2	2.734	-0.196	1.216	Silty Sand
3	Rou. 1-3	213.6	3.202	-0.364	1.201	Silty Sand	13	Rou. 3-5	10.27	2.884	0.240	1.541	Silt
4	Rou. 1-4	7.857	4.409	-0.267	1.858	Silt	14	Rou. 3-6	37.48	3.616	-0.285	0.639	Sandy Silt
5	Rou. 2-1	31.76	7.081	-0.089	0.945	Sandy Silt	15	Rou. 4-1	48.39	5.907	-0.610	1.054	Silty Sand
6	Rou. 2-2	23.23	6.040	0.053	0.974	Sandy Silt	16	Rou. 4-2	65.76	3.304	-0.694	2.073	Silty Sand
7	Rou. 2-3	29.74	5.567	0.262	0.802	Sandy Silt	17	Rou. 4-3	19.49	3.676	0.420	0.760	Sandy Silt
8	Rou. 2-4	49.92	3.911	-0.524	0.639	Silty Sand	18	Rou. 4-4	26.54	6.104	-0.083	0.976	Sandy Silt
9	Rou. 3-1	91.83	3.979	-0.571	0.635	Silty Sand							
10	Rou. 3-2	19.22	3.437	0.381	0.814	Sandy Silt							

Supplementary Table 2. Results of calculating LDFs, classifying sedimentary environments according to Baiyegunhi et al., (2020)

Sample	Router sample 1								Router sample 2					
	Rou. 1-1		Rou. 1-2		Rou. 1-3		Rou. 1-4		Rou. 2-1		Rou. 2-2		Rou. 2-3	
Y_1	-1.22	Littoral	-2.04	Littoral	1.25	Littoral	-11.8	Shallow agitated water	-4.55	Shallow agitated water	-6.63	Shallow agitated water	-5.89	Shallow agitated water
Y_2	237.11	Shallow marine	282.02	Shallow marine	174	Shallow marine	289.31	Shallow marine	282.56	Shallow marine	272.53	Shallow marine	252.23	Shallow marine
Y_3	-23.48	lacustrine or deltaic	-25.41	Lacustrine or deltaic	-15.8	Lacustrine or deltaic	-17.98	Lacustrine or deltaic	-23.71	Lacustrine or deltaic	-20.88	lacustrine or deltaic	-18.93	lacustrine or deltaic

Sample	Router sample 1								Router sample 2					
	Rou. 1-1		Rou. 1-2		Rou. 1-3		Rou. 1-4		Rou. 2-1		Rou. 2-2		Rou. 2-3	
Y_4	9.6	Turbidity current	7.52	Turbidity current	9.74	Turbidity current	15.81	deltaic deposition	8.05	Turbidity current	7.67	Turbidity current	5.14	Turbidity current
Sample	Router sample 2		Router sample 3											
	Rou. 2-4		Rou. 3-1		Rou. 3-2		Rou. 3-3		Rou. 3-4		Rou. 3-5		Rou. 3-6	
Y_1	-7.25	Shallow agitated water	-4.13	Shallow agitated water	-10.43	Shallow agitated water	-12.09	Shallow agitated water	-2.24	Littoral	-12.62	Shallow agitated water	-8.64	Shallow agitated water
Y_2	218.3	Shallow marine	206.93	Shallow marine	214.46	Shallow marine	224.2	Shallow marine	169.63	Shallow marine	228	Shallow marine	212.99	Shallow marine
Y_3	-18.54	Lacustrine or deltaic	-19.24	lacustrine or deltaic	-12.08	Lacustrine or deltaic	-9.73	Lacustrine or deltaic	-12.73	Lacustrine or deltaic	-10.26	lacustrine or deltaic	-16.25	lacustrine or deltaic
Y_4	9.24	Turbidity current	8.88	Turbidity current	5.14	Turbidity current	9.91	Deltaic deposition	9.39	Turbidity current	10.69	deltaic deposition	7.97	Turbidity current
Sample	Router sample 4													
	Rou. 4-1		Rou. 4-2		Rou. 4-3		Rou. 4-4							
Y_1	-4.09	Shallow agitated water	-2.62	Littoral	-10.09	Shallow agitated water	-6.16	Shallow agitated water						
Y_2	267.33	Shallow marine	225.68	Shallow marine	218.81	Shallow marine	273	Shallow marine						
Y_3	-24.14	Lacustrine or deltaic	-17.28	Lacustrine or deltaic	-12.74	Lacustrine or deltaic	-21.73	Lacustrine or deltaic						
$_4$	11.81	Deltaic deposition	17.78	Deltaic deposition	4.54	Turbidity current	8.45	Turbidity current						

RESULTS

Sedimentary characteristics of the study area

The analysis of the eighteen samples revealed that the sediments in the study area consisted of silty sand, sandy silt, silt, and clay with poor to very poor sorting (Supplementary Table 1). The sediment grain sizes ranged from 0.138 (Sample Rou.1-4) to 1,337.481 µm (Sample Rou.1-3). The graph depicting the relationship between particle size and the frequency of occurrence illustrates that within the entire sample set, there are local maxima within the following particle size ranges: 0.17–0.55 µm; 5–15 µm; 69–129 µm; and 184–580 µm. These ranges correspond to clay sediment, fine to medium silt, fine sand, and fine to medium sand (Figure 2).

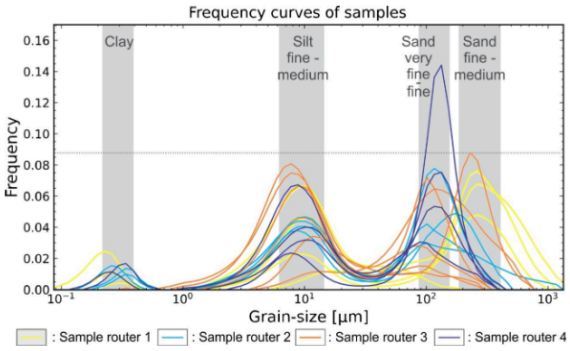

Figure 2. Characteristics of surface sediment grain size in the study area

Analysis results of LDFs

The results of calculating LDFs, as presented in Supplementary Table 2, demonstrate that the indices Y_1, Y_2, Y_3, and Y_4 exhibit fluctuations within the following ranges: -12.62 to 1.25, 169.63 to 289.31, -25.24 to -9.73, and 4.54 to 17.78, respectively. Based on the results of calculations for all samples within the study area, when index Y_2 exceeds -63.365, and Y_3 is less than -7.42, this suggests a sediment accumulation environment characterized as a shallow marine environment or lagoon, lacustrine, or deltaic environment. Sample Route 1 contains 3 out of 4 samples with a Y_1 index greater than -2.74, corresponding to a coastal marine accumulating environment (littoral). The remaining samples with a Y_1 index above -2.74 belong to the agitated shallow water environment, accounting for 13 out of 18 samples. The Y_4 index exhibits a similar pattern to Y_1, with 13 out of 18 samples falling into the sedimentary environment associated with turbidity currents. In contrast, the remaining samples are related to the deltaic deposition environment.

End-member modelling analysis

Normalizing the input data indicates that the model exhibits the highest stability when utilizing weight transformation with a value of l = 0.03, resulting in a mean total explained variance of mRt = 0.668 (Figure 3a). The determination of the optimal number of endmembers is based on the stability of the relationship between the number of end members (q), weights (l), and the total variance of the model (R_t^2). The results suggest that a choice of q = 4 corresponds to a stable relationship with weight l in the range of 0–0.05, resulting in R_t^2 = 0.72 (Figure 3b and 3c). For cases where q = 2 or q = 3, the total extracted variance is smaller than when q = 4.

In contrast, when q = 5 or q = 6, a larger total extracted variance is achieved, but the relationship between q and l is less stable compared to the case with q = 4 (Figure 3b).

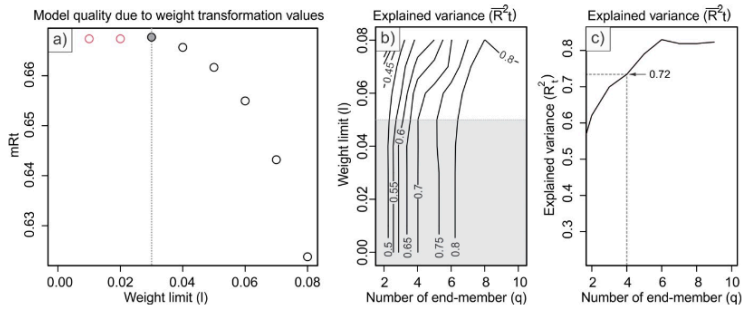

Figure 3. The relationship between the weight variable value parameters (l), the number of final members (q), and the variance (R_t^2)

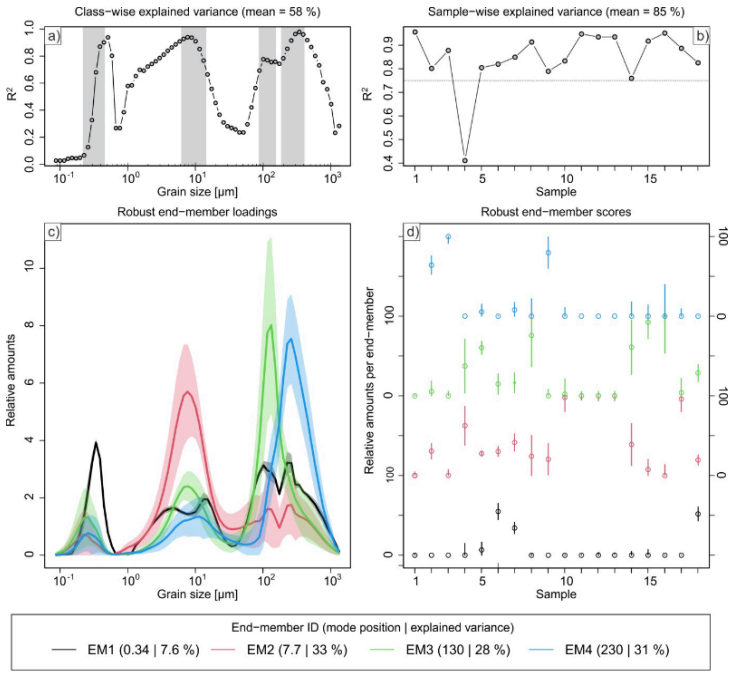

Figure 4. EMMAgeo model results

Figure 4 displays the outcomes of the EMMAgeo model applied to the sample set within the study area. The last four members of EM1, EM2, EM3, and EM4 have been identified. The model's fit for the grain sizes and samples is illustrated by the mean extracted variance values of 0.58 and 0.85, respectively (Figures 4a and 4b).

Figure 4c represents the statistical result of reducing the correlation dimension of sediment grain size for the entire sample set to 4 EM, converted to total variance R_1^2 = 100%, including EM1 = 7.6%, EM2 = 33%, EM3 = 28%, and EM4 = 31%. Accordingly, the dominant modes for each end member (EMs) are 0.34 µm (clay), 7.7 µm (fine silt), 130 µm (fine sand), and 230 µm (fine sand), respectively. In each EM, secondary peaks represent the sub-modes in the sedimentation process. These sub-modes play a secondary role and are shown as secondary factors related to the regional sediment distribution laws. The level of contribution of each EM in the samples expressed in scores (Figure 4d) shows that most of the samples are mainly contributed by EM2 and EM3.

DISCUSSION

Sedimentary environment of the study area

The results of sediment sample classification align with previous research on sediments within the study area [32–33, 39, 41]. The sediment deposition environments, as classified based on the research [10] presented in Figure 5, exhibit wide dispersion ranges that reflect complex sediment accumulation environments. However, a discernible influence of river or wave processes is not observed. Most of sediments within the study area are categorized within the fluvial and marine distribution field and are associated with coastal dunes (related to littoral) (Figure 5a). This classification is appropriate since the sediment samples were primarily collected between islands far from the river mouth and at depths ranging from 8 to 14 meters. Consequently, the sediment accumulation environment is less directly impacted by wave and river processes but is primarily influenced by tidal and coastal currents.

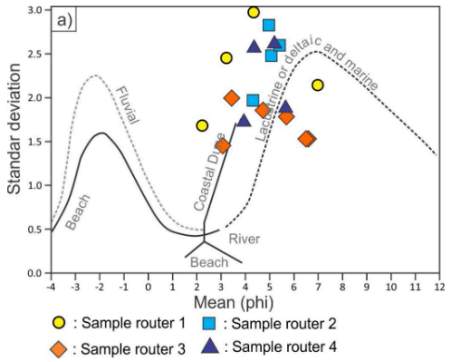

Figure 5. Mean size relationship chart and standard deviation comparing the sediment accumulation environment in the study area with the sediment accumulation environment from the studies of Folk and Ward (1957) [3]; Baiyegunhi et al. (2020) and Selvaraj and Mohan (2003) [8, 10]

The Linear Discrimination Function (LDF) graph depicted in Figure 6 reveals that the relationship between Y_1 and Y_2 reflects the sediment accumulation environment in the study area, primarily characterized as a shallow sea, with the majority falling into the category of

shallow agitated waters. Samples from Line 1 are predominantly situated in coastal waters (Littoral) (as shown in Figure 6a). The relationship diagrams $Y_2 - Y_3$ and $Y_3 - Y_4$ show that the sediments in the study area are primarily deltaic sediments originating from ancient sedimentary rocks, eroded and deposited by dynamic processes in agitated water environments and turbidity currents (as depicted in Figures 6b and 6c). Studies on sediments in neighboring areas have suggested that sediment sources from rivers are minimal, primarily derived from erosion around the bay [39, 42]. Consequently, the results indicate that the river process less influences sedimentation in the study area. Instead, the accumulation process occurs in shallow coastal marine environments, with the primary source of material being products from the erosion of ancient sedimentary rocks around the bay. These materials are predominantly transported in shallow agitated water and (or) turbidity currents.

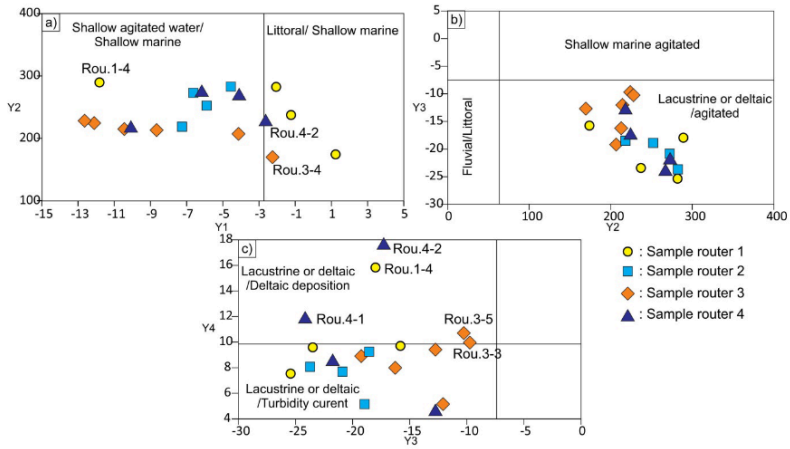

Figure 6. Linear discriminant function graph. Characteristics of the accumulation environment are based on Sahu (1964) [5] and Baiyegunhi et al. (2020) [10]

Spatial distribution of End-members

End members EM1 and EM2 correspond to clay and fine silt, likely representing suspended sediments transported by currents. EM1, being smaller in size, tends to deposit under low-energy conditions and is not commonly distributed throughout the study area. As shown in Figure 7a, EM1 is found in only 4 sample locations, with 3 of them situated between small islands in sample line No. 2, having contribution scores ranging from 10% to 52%. The highest score of 55% is recorded at a sample location outside the bay in sample line 4, at a depth of 11 m, where the topographic gradient undergoes significant changes. In contrast, EM2 is present in 15 out of 18 sample locations, indicating that the flow regime predominantly influences the sediment accumulation process in the study area (Figure 7b). However, the contribution index of EM2 is not uniform across the region, with high values at sites along line 3 and one location on line 4 (Figure 7b). Notably, locations where EM1 appears tend to have lower EM2 scores. These differences and the contribution scores at sample locations indicate that the flow energy is heterogenous across the study area, with locations sandwiched between islands on sample line 2 experiencing the lowest flow energy, followed by the Cai Chien and Vinh

Thuc island areas on sample line 3, and the highest flow energy observed in the shallow sea along the coast of Van Don Peninsula on sample line number 1. The changes in end members (EMs) outside Bai Tu Long Bay are complex. It is worth noting that the sampling occurred in March 2022 at the end of the dry season. According to research by Nguyen (2013) [38], during the dry season, due to the influence of monsoons, tidal regimes, and wind-driven currents, most suspended materials from the Hainan Strait are transported eastward into the open sea outside Bai Tu Long Bay (Western of Coto island). Additionally, when comparing the sampling locations with the February flow regime map in the Vietnam National Atlas [43], it becomes evident that Rou.4-3 and Rou.4-4 fall within a localized counterclockwise flow vortex range. This condition might promote substantial accumulation when EM1 and EM2 scores are relatively high. However, at locations Rou.4-1 and Rou.4-2, the accumulation of suspended material is nearly absent, with EM3 having a significantly high contribution score and the sediment composition primarily consisting of fine-grained sand. These two sample points align with the research results of previous authors [32–33] in that they are located in an erosion area. In conclusion, the accumulation process in the outer area of Bai Tu Long Bay is quite complicated, warranting further research.

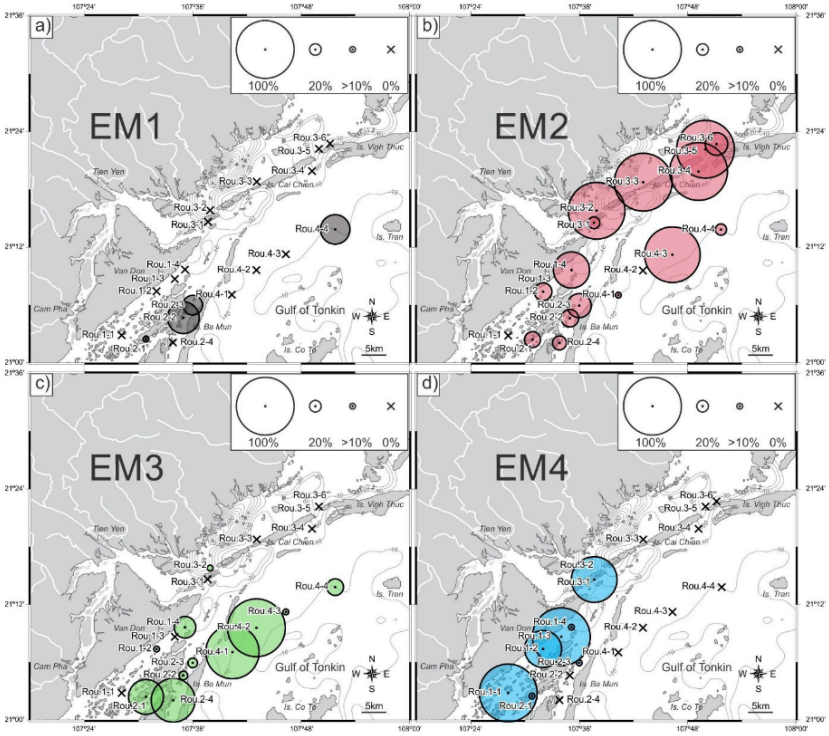

Figure 7. Spatial distribution of the content of End-members in the study area

End members EM3 and EM4, with grain sizes at the peaks of 130 µm and 230 µm, correspond to fine sand sediments that are less easily transported in suspension by currents and are primarily formed through tidal and wave processes. As shown in Figures 7c and 7d, EM3 is observed throughout most of the study area, whereas EM4, with coarser grain sizes, is primarily concentrated along the coast of the Van Don Peninsula. While this study did not sample sediments in the Tien Yen and Ka Long estuary areas, several previous studies have indicated the existence of similar sediments [32, 34, 39, 42]. Dang et al., (2020) [34] suggested that fine sand in the study area is formed through the erosion of coastal sands. This area is characterized by strong dynamics, particularly influenced by tides, especially during the ebb tide [32]. In the intertidal zones of the bay, dominant tidal currents give rise to sand dunes connecting the islands. In some funnel-shaped estuaries (e.g., Tien Yen River, Ka Long River), these dunes are distributed parallel to the riverbed. Although values of EM3 and EM4 are present at most sample locations in the study area, the heterogeneity in their distribution characteristics indicates that the influence of the tidal process on the area is not uniform. Along the coast of the Van Don Peninsula, where EM4 is primarily concentrated, it is considered an area more strongly affected by tides than other regions.

The results of the spatial distribution of Endmembers in the study area indicate a division into two regions: lower environmental energy conditions in the North and higher environmental energy conditions in the South. The North exhibits high EM2 values, while the South shows high EM3 and EM4 values.

CONCLUSION

The coastal area extending from Van Don to Tien Yen - Ha Coi is characterized by relatively complex sediments with poor selectivity, encompassing four sediment types: silty sand, sandy silt, silt, and clay. These sediments in the study area originated in a shallow coastal marine environment, with the material source attributed to erosion occurring around the bay. The transport mechanism mainly involves disturbances in shallow agitated water and/or turbidity currents.

The statistical results of particle size composition using the EMMAgeo model have identified four main members (EMs) corresponding to four distinct sediment types: clay, fine silt, and fine sand of varying sizes. These sediments are the major factors and statistically essential components of the whole sediment composition within the study area. Fine-silt sediments are dispersed uniformly across the research area, but their contribution gradually diminishes from north to south, commensurate with a gradual increase in environmental energy for sediment accumulation. Notably, the coastal area along the Van Don Peninsula has the highest environmental energy for sediment accumulation, resulting in poor sediment accumulation primarily comprised of fine-grained sand. In addition, the locations situated between islands experience the lowest environmental energy for sediment accumulation, where the sediment is predominantly clay sand. In the outer part of the bay, two contrasting accumulation environments exist. The northern region, near Co To Island, is characterized by high sediment accumulation. Meanwhile, the western region features erosion and low sediment accumulation.

Acknowledgements: This study was funded by the Basic Investigation Mission of the Vietnam Academy of Science and Technology, number UQDTCB.01/22–23.

REFERENCES

[1] Hein, C. J., and Ashton, A. D., 2020. Long-term shoreline morphodynamics: processes and preservation of environmental signals. *Sandy Beach Morphodynamics*, 487–531. https://doi.org/10.1016/B978-0-08-102927-5.00021-7

[2] Hendriks, H. C. M., Van Prooijen, B. C., Aarninkhof, S. G. J., and Winterwerp, J. C., 2020. How human activities affect the fine sediment distribution in the Dutch

Coastal Zone seabed. *Geomorphology*, *367*, 107314. https://doi.org/10.1016/j.geomorph.2020.107314

[3] FolkRL, W. C., 1957. A study in the significance of grain size parameters. *Journal of Sedimentary Petrology*, *27*, 3–27. https://doi.org/10.1306/74D70646-2B21-11D7-8648000102C1865D

[4] Friedman, G. M., 1967. Dynamic processes and statistical parameters compared for size frequency distribution of beach and river sands. *Journal of Sedimentary Research*, *37*(2), 327–354. https://doi.org/10.1306/74D716CC-2B21-11D7-8648000102C1865D

[5] Sahu, B. K., 1964. Depositional mechanisms from the size analysis of clastic sediments. *Journal of Sedimentary Research*, *34*(1), 73–83. https://doi.org/10.1306/74D70FCE-2B21-11D7-8648000102C1865D

[6] Ghosh, S. K., and Chatterjee, B. K., 1994. Depositional mechanisms as revealed from grain-size measures of the palaeoproterozoic Kolhan siliciclastics, Keonjhar District, Orissa, India. *Sedimentary Geology*, *89*(3–4), 181–196. https://doi.org/10.1016/0037-0738(94)90093-0

[7] Dietze, M., Dietze, E., Lomax, J., Fuchs, M., Kleber, A., and Wells, S. G., 2016. Environmental history recorded in aeolian deposits under stone pavements, Mojave Desert, USA. *Quaternary Research*, *85*(1), 4–16. doi: 10.1016/j.yqres.2015.11.007

[8] Selvaraj, K., and Mohan, V. R., 2003. Textural variation and depositional environments of innershelf sediments, off Kalpakkam, southeast coast of India. *Journal-Geological Society of India*, *61*(4), 449–462.

[9] Li, T., and Li, T. J., 2018. Sediment transport processes in the Pearl River Estuary as revealed by grain-size end-member modeling and sediment trend analysis. *Geo-Marine Letters*, *38*, 167–178. https://doi.org/10.1007/s00367-017-0518-2

[10] Baiyegunhi, T. L., Liu, K., Gwavava, O., and Baiyegunhi, C., 2020. Textural characteristics, mode of transportation and depositional environment of the Cretaceous sandstone in the Bredasdorp Basin, off the south coast of South Africa: Evidence from grain size analysis. *Open Geosciences*, *12*(1), 1512–1532. https://doi.org/10.1515/geo-2020-0135

[11] Alexander, C. R., DeMaster, D. J., and Nittrouer, C. A., 1991. Sediment accumulation in a modern epicontinental-shelf setting: the Yellow Sea. *Marine Geology*, *98*(1), 51–72. https://doi.org/10.1016/0025-3227(91)90035-3

[12] Vandenberghe, J., 2013. Grain size of fine-grained windblown sediment: A powerful proxy for process identification. *Earth-Science Reviews*, *121*, 18–30. doi: 10.1016/j.earscirev.2013.03.001

[13] Vandenberghe, J., Lu, H., Sun, D., van Huissteden, J. K., and Konert, M., 2004. The late Miocene and Pliocene climate in East Asia as recorded by grain size and magnetic susceptibility of the Red Clay deposits (Chinese Loess Plateau). *Palaeogeography, Palaeoclimatology, Palaeoecology*, *204*(3–4), 239–255. https://doi.org/10.1016/S0031-0182(03)00729-6

[14] Tamura, T., Horaguchi, K., Saito, Y., Nguyen, V. L., Tateishi, M., Ta, T. K. O., Nanayama, F., and Watanabe, K., 2010. Monsoon-influenced variations in morphology and sediment of a mesotidal beach on the Mekong River delta coast. *Geomorphology*, *116*(1–2), 11–23. https://doi.org/10.1016/j.geomorph.2009.10.003

[15] Tamura, T., Nguyen, V. L., Ta, T. K. O., Bateman, M. D., Gugliotta, M., Anthony, E. J., Nakashima, R., and Saito, Y., 2020. Long-term sediment decline causes ongoing shrinkage of the Mekong megadelta, Vietnam. *Scientific Reports*, *10*(1), 8085. https://doi.org/10.1038/s41598-020-64630-z

[16] Nguyen, V. L., Ta, T. K. O., and Tateishi, M., 2000. Late Holocene depositional environments and coastal evolution of the Mekong River Delta, Southern Vietnam. *Journal of Asian Earth Sciences*, *18*(4), 427–439. https://doi.org/10.1016/S1367-9120(99)00076-0

[17] Mathers, S., and Zalasiewicz, J., 1999. Holocene sedimentary architecture of the Red River delta, Vietnam. *Journal of Coastal Research*, 314–325.

[18] Dietze, E., Wünnemann, B., Hartmann, K., Diekmann, B., Jin, H., Stauch, G., Yang, S., and Lehmkuhl, F., 2013. Early to mid-Holocene lake high-stand sediments at Lake Donggi Cona, northeastern Tibetan Plateau, China. *Quaternary Research*, *79*(3), 325–336. doi: 10.1016/j.yqres.2012.12.008

[19] Zhang, X., Ji, Y., Yang, Z., Wang, Z., Liu, D., and Jia, P., 2016. End member inversion of surface sediment grain size in the South Yellow Sea and its implications for dynamic sedimentary environments. *Science China Earth Sciences*, *59*, 258–267. https://doi.org/10.1007/s11430-015-5165-8

[20] Zhang, K., Li, A., Zhang, J., Lu, J., and Wang, H., 2020. Seasonal variations in the surficial sediment grain size in the East China Sea continental shelf and their implications for terrigenous sediment transport. *Journal of Oceanography*, *76*, 1–14. https://doi.org/10.1007/s10872-019-00523-8

[21] Liang, J., Liu, J., Xu, G., and Chen, B., 2020. Grain-size characteristics and net transport patterns of surficial sediments in the Zhejiang nearshore area, East China Sea. *Oceanologia*, *62*(1), 12–22. https://doi.org/10.1016/j.oceano.2019.06.002

[22] Flemming, B. W., 2007. The influence of grain-size analysis methods and sediment mixing on curve shapes and textural parameters: implications for sediment trend analysis. *Sedimentary Geology*, *202*(3), 425–435. https://doi.org/10.1016/j.sedgeo.2007.03.018

[23] Flemming, B. W., 1988. Process and patterns of sediment mixing in a microtidal coastal lagoon along the west coast of South Africa. In *Symposium on clastic tidal deposits. Extended versions of papers*, pp. 275–288.

[24] Weltje, G. J., 1997. End-member modeling of compositional data: Numerical-statistical algorithms for solving the explicit mixing problem. *Mathematical Geology*, *29*, 503–549. https://doi.org/10.1007/BF02775085

[25] Weltje, G. J., and Prins, M. A., 2003. Muddled or mixed? Inferring palaeoclimate from size distributions of deep-sea clastics. *Sedimentary Geology*, *162*(1–2), 39–62. https://doi.org/10.1016/S0037-0738(03)00235-5

[26] Van Hateren, J. A., Prins, M. A., and Van Balen, R. T., 2018. On the genetically meaningful decomposition of grain-size distributions: A comparison of different end-member modelling algorithms. *Sedimentary geology*, *375*, 49–71. https://doi.org/10.1016/j.sedgeo.2017.12.003

[27] Dietze, E., Hartmann, K., Diekmann, B., IJmker, J., Lehmkuhl, F., Opitz, S., Stauch, G., Wünnemann, B., and Borchers, A., 2012. An end-member algorithm for deciphering modern detrital processes from lake sediments of Lake Donggi Cona, NE Tibetan Plateau, China. *Sedimentary Geology*, *243*, 169–180. https://doi.org/10.1016/j.sedgeo.2011.09.014

[28] Ha, H. J., Chang, T. S., and Ha, H. K., 2021. Using end-member analysis to determine sediment dispersal and depositional processes on the Heuksan mud belt, southwest Korean shelf. *Geo-Marine Letters*, *41*, 1–13. https://doi.org/10.1007/s00367-020-00672-6

[29] López-González, N., Alonso, B., Juan, C., Ercilla, G., Bozzano, G., Cacho, I., Casas, D., Palomino, D., Vázquez, J. T., Estrada, F., Bárcenas, P., D'Acremont, E., Gorini, C., and Moumni, B. E., 2019. 133,000 Years of sedimentary record in a contourite drift in the Western Alboran Sea: sediment sources and paleocurrent reconstruction. *Geosciences*, *9*(8), 345. https://doi.org/10.3390/geosciences9080345

[30] Dong, M. D., Poizot, E., Cuong, D. H., Anh, L. D., Hung, D. Q., Thuy Huong, T. T., Diep, N. V., and Huong, N. B., 2023. Transport trend of recent sediment within the nearshore seabed of Hai Hau, Nam Dinh Province, Southwest Red River Delta.

Frontiers in Earth Science, *11*, 1099730. https://doi.org/10.3389/feart.2023.1099730

[31] Li, T., Cai, G., Wang, C., Liang, K., Ma, S., and Luo, W., 2021. Quantifying clay mineral sources in marine sediments by using end-member mixing analysis. *Geo-Marine Letters*, *41*, 1–11. https://doi.org/10.1007/s00367-020-00674-4

[32] Nguyen, N. A., 2014. Characteristics and dynamic evolution of surface sedimentary formations in coastal shallow seas Hai Phong - Quang Ninh. *Thesis of Doctor Geology*. (in Vietnamese)

[33] Tran, N., 2010. 2010. Marine and petroleum geology. *Vietnam National University Press, Hanoi*, 334 p. (in Vietnamese).

[34] Dang, H. N., Duong, T. N., and Tran, D. T., 2020. Intertidal zone in the north of Viet Nam: Features and potential development. *Publishing House for Science and Technology*, 260 p. (in Vietnamese).

[35] Nguyen, M. H., 2010. Changes in coastal and estuary of Vietnam. *Publishing House for Science and Technology*, 233 p. (in Vietnamese).

[36] Vu, V. P., Nguyen, H., Duong, T. N., and Vu, L. P., 2009. Explanatory report on mapping the marine geomorphology of Tien Yen - Ha Coi bay, scale 1:50,000. *Center for Marine Geology and Minerals.* (in Vietnamese).

[37] Nguyen, N. T., 1984. Tides in the waters of Vietnam. *Publishing House for Science and Technology.*

[38] Nguyen, N. M., 2013. Tidal characteristics of the Gulf of Tonkin. *Doctoral dissertation, Université Paul Sabatier-Toulouse III*.

[39] Vuong, B. V., Liu, Z., Thanh, T. D., Huh, C. A., Nhon, D. H., Ve, N. D., and Huy, D. V., 2016. Intital Results of Study on Sedimentation Rate, Sediment Sources to Ha Long Bay: Evidence from the ^{210}Pb and ^{137}Cs Radiotracer, Vietnam Joural of Marine Science and Technology, *16*(1), 54–63. https://doi.org/10.15625/1859-3097/16/1/6527 (in Vietnamese).

[40] Dietze, E., and Dietze, M., 2019. Grain-size distribution unmixing using the R package EMMAgeo. *E&G Quaternary Science Journal*, *68*(1), 29–46. https://doi.org/10.5194/egqsj-68-29-2019

[41] Nhon, D. H., Van Thao, N., Thanh, T. D., Ve, N. D., Van Vuong, B., Thuy, L. T. B., Loan, B. T. T., Chien, H. T., and Nghi, D. T., 2023. Characteristic and distribution of grain sizes and minerals in sediments from the Vietnamese Gulf of Tonkin. *Vietnam Journal of Science, Technology and Engineering*, *65*(2), 88–96. https://doi.org/10.31276/VJSTE.65(2).88-96

[42] Nhon, D. H., Luu, N. T. M., Thuy, L. T. B., Nam, N. N., Hoang, N. H., and Quan, B. M., 2019. Mineral compositions and grain sizes of sediments in intertidal zone in Northern Vietnam. *Vietnam Journal of Marine Science and Technology*, *19*(3A), 63–75. https://doi.org/10.15625/1859-3097/19/3A/14292 (in Vietnamese).

[43] Nguyen, V. C., et al., 1996. The Vietnam National Atlas program. *Vietnam Publishing House of Natural Resources, Environment and Cartography*, 163 p. (in Vietnamese).